

Electroweak Couplings of the Higgs Boson at a Multi-TeV Muon Collider

Tao Han,^a Da Liu,^b Ian Low^{c,d} and Xing Wang^e

^a*Department of Physics and Astronomy, University of Pittsburgh, Pittsburgh, PA 15217, USA*

^b*Center for Quantum Mathematics and Physics (QMAP), University of California, Davis, CA 95616, USA*

^c*Department of Physics and Astronomy, Northwestern University, Evanston, IL 60208, USA*

^d*High Energy Physics Division, Argonne National Laboratory, Lemont, IL 60439, USA*

^e*Department of Physics, University of California-San Diego, La Jolla, CA 92093, USA*

ABSTRACT: We estimate the expected precision at a multi-TeV muon collider for measuring the Higgs boson couplings with electroweak gauge bosons, HVV and $HHVV$ ($V = W^\pm, Z$), as well as the trilinear Higgs self-coupling HHH . At very high energies both single and double Higgs productions rely on the vector-boson fusion (VBF) topology. The outgoing remnant particles have a strong tendency to stay in the very forward region, leading to the configuration of the “inclusive process” and making it difficult to isolate ZZ fusion events from the WW fusion. In the single Higgs channel, we perform a maximum likelihood analysis on HWW and HZZ couplings using two categories: the inclusive Higgs production and the 1-muon exclusive signal. In the double Higgs channel, we consider the inclusive production and study the interplay of the trilinear HHH and the quartic $VVHH$ couplings, by utilizing kinematic information in the invariant mass spectrum. We find that at a centre-of-mass energy of 10 TeV (30 TeV) with an integrated luminosity of 10 ab^{-1} (90 ab^{-1}), one may reach a 95% confidence level sensitivity of 0.073% (0.023%) for WWH coupling, 0.61% (0.21%) for ZZH coupling, 0.62% (0.20%) for $WWHH$ coupling, and 5.6% (2.0%) for HHH coupling. For dim-6 operators contributing to the processes, these sensitivities could probe the new physics scale Λ in the order of $1 - 10$ ($2 - 20$) TeV at a 10 TeV (30 TeV) muon collider.

Contents

1	Introduction	1
2	Higgs Boson Production at a High-energy Muon Collider	4
3	VVH Couplings	5
3.1	Inclusive channel	6
3.2	Exclusive 1μ channel	8
3.3	Two-parameter likelihood fit of κ_W and κ_Z	10
4	HHH and $WWHH$ Couplings	11
5	Discussion and Conclusion	13

1 Introduction

The discovery of the Higgs boson at the CERN Large Hadron Collider (LHC) opens a new avenue in particle physics. On the one hand, the existence of the Higgs boson completes the particle spectrum in the Standard Model (SM) and provides a self-consistent mechanism in quantum field theory for mass generation of elementary particles. On the other hand, the SM does not address the underlying mechanism for the electroweak symmetry breaking (EWSB) and thus fails to understand the stability of the weak scale with respect to the Planck scale. In order to gain further insight for those fundamental questions, it is of high priority to study the Higgs boson properties to high precision in the hope to identify hints for new physics beyond the SM.

In the SM, the Higgs sector is constructed from a complex scalar doublet Φ . After the EWSB, the neutral real component is the Higgs boson excitation H and the other three degrees of freedom become the longitudinal components of the massive gauge bosons. As such, studying the Higgs-gauge boson couplings would be the most direct probe to the underlying mechanism of the electroweak symmetry breaking. After the EWSB, the Higgs sector can be parameterized as

$$\mathcal{L} \supset \left(M_W^2 W_\mu^+ W^{-\mu} + \frac{1}{2} M_Z^2 Z_\mu Z^\mu \right) \left(\kappa_V \frac{2H}{v} + \kappa_{V2} \frac{H^2}{v^2} \right) - \frac{m_H^2}{2v} \left(\kappa_3 H^3 + \frac{1}{4v} \kappa_4 H^4 \right), \quad (1.1)$$

where $v = 246$ GeV is the vacuum expectation value of the Higgs field and $\kappa_i = 1$ for the SM couplings at tree-level. This “ κ -scheme” is a convenient phenomenological parameterization of deviations from the SM expectations, which is suitable for the exploratory nature of the

present study. Here it is made implicit that $\kappa_V = \kappa_W = \kappa_Z$. This is the prediction of the tree-level custodial SU(2) invariance [1], which is an accidental symmetry of the SM. This has been verified to a good accuracy by precision EW measurements [2]. Nevertheless, in our fit we wish to be more general and will not be assuming a correlated κ_W and κ_Z .

A fully consistent and theoretically-sound framework would utilize effective field theories (EFT), by augmenting the SM Lagrangian with higher dimensional operators from integrating out the heavier states [3]. While a systematic account for the effects of the higher dimensional operators is much more involved and beyond the scope of the current work, we would like to consider the following two operators for the purpose of illustration [4, 5]

$$\mathcal{O}_H = \frac{c_H}{2\Lambda^2} \partial_\mu (\Phi^\dagger \Phi) \partial^\mu (\Phi^\dagger \Phi) , \quad \mathcal{O}_6 = -\frac{c_6 \lambda}{\Lambda^2} (\Phi^\dagger \Phi)^3 , \quad (1.2)$$

where Λ is the cutoff scale where new physics sets in, and λ is the quartic coupling parameter in front of $(H^\dagger H)^2$ term in the SM Higgs potential. At the dimension-six level these are the two operators that are most relevant for our study. An additional operator, $\Phi^\dagger \Phi (D_\mu \Phi)^\dagger (D^\mu \Phi)$, can be removed by a suitable field-redefinition [5]. The resulting shifts $\Delta\kappa_i \equiv \kappa_i - 1$ in Eq. (1.1) are¹

$$\begin{aligned} \Delta\kappa_V &= -\frac{c_H}{2} \frac{v^2}{\Lambda^2} , & \Delta\kappa_{V2} &= -2c_H \frac{v^2}{\Lambda^2} , \\ \Delta\kappa_3 &\approx -\frac{3c_H}{2} \frac{v^2}{\Lambda^2} + c_6 \frac{v^2}{\Lambda^2} , & \Delta\kappa_4 &\approx -\frac{25}{9} c_H \frac{v^2}{\Lambda^2} + 6c_6 \frac{v^2}{\Lambda^2} , \end{aligned} \quad (1.3)$$

We see that deviations in the VVH and $VVHH$ ($V = W^\pm, Z$) couplings are correlated and controlled by the same operator \mathcal{O}_H . However, the precision we are expecting is high and could potentially be sensitive to effects of dimension-8 operators, in which case the correlation may be modified. On the other hand, the Higgs trilinear self-coupling κ_3 is among the most important interactions to be tested in the Higgs sector – it governs the shape of the Higgs potential and, consequently, the nature of the electroweak symmetry breaking. In addition, κ_3 controls the strength of the electroweak phase transition, which is important for understanding the cosmological evolution of the early universe as well as the origin of the observed matter-anti-matter asymmetry in the current universe [7–9]. Precise measurements of these couplings will provide insights on how nature works at the shortest distance scale ever probed by mankind. Needless to say, should deviations from the SM predictions be observed, it would completely revolutionize our understanding of the physical laws of nature.

With the great success of the LHC program, we have achieved the measurement of the VVH to $\mathcal{O}(5\%)$ accuracy [10, 11], which will be further improved by roughly a factor of two with the high-luminosity LHC upgrade [12]. In e^+e^- collisions at the International Linear Collider (ILC) [13, 14], the proposed Higgs factories [15–17] and the CLIC [18, 19], sub-percent level accuracies for WWH of $\mathcal{O}(0.6\% - 1.2\%)$ and ZZH of $\mathcal{O}(0.2\% - 0.5\%)$ could

¹Interestingly, in most cases there is a positivity constraint on $c_H > 0$, thereby reducing the VVH and $VVHH$ coupling strengths [6].

be achievable. However, the trilinear HHH and quartic $VVHH$ couplings are still difficult to measure to an informative level without a very high energy collider [20, 21]. At a 100 TeV hadron collider such as the SPPC or FCC_{hh}, the trilinear Higgs self-coupling could be measured with $\mathcal{O}(5\%)$ uncertainty [22, 23]. Recently, an attempt was made to determine the quartic Higgs self-coupling at a high-energy muon collider [24]. In the EFT language, the precision to which one could measure the Higgs couplings can be translated into constraints on the scale suppressing dimension-6 operators, which is indicative of the scale where new physics becomes important. A figure of merit is when $\Lambda \sim 1$ TeV which, generally speaking, would induce a corresponding deviation in the Higgs couplings of the order [25]

$$\mathcal{O}\left(\frac{v^2}{\Lambda^2}\right) \sim \mathcal{O}(5\%) \quad \text{for } \Lambda \sim 1 \text{ TeV} . \quad (1.4)$$

Therefore, in order to probe new physics scale above 1 TeV, it is important to be able to reach a precision level of 5% or less. In addition, in a lepton collider a truly model-independent determination of the trilinear HHH coupling requires simultaneously measuring the 4-point $VVHH$ coupling, which is difficult to access at low energies and without sufficiently high statistics.

Recently, there has been a renewed interest to consider a muon collider with a very high centre-of-mass (CM) energy in the tens of TeV [26–31]. While the previous discussions for a muon collider were focused on a Higgs factory operating at the SM Higgs resonance [32, 33], a collider operating at a multi-TeV regime would certainly lead us to a new territory at the energy frontier. Such a multi-TeV muon collider offers a unique opportunity to probe the electroweak couplings of the Higgs boson, including VVH , HHH and $VVHH$ couplings. The possible CM energy under discussion ranges from 3 TeV to 30 TeV, with a representative benchmark target at 10 TeV or higher. Very high luminosities are also envisioned, with the scaling relation as [26]

$$\text{Lumi.} > \frac{5 \text{ years}}{\text{time}} \left(\frac{\sqrt{s}}{10 \text{ TeV}} \right)^2 2 \cdot 10^{35} \text{ cm}^{-2}\text{s}^{-1}. \quad (1.5)$$

This will yield to an integrated luminosity of $\mathcal{O}(10)$ ab⁻¹ at $\sqrt{s} = 10$ TeV and $\mathcal{O}(90)$ ab⁻¹ at $\sqrt{s} = 30$ TeV, which would take us to a remarkable new energy frontier, and offer great potential to study the Higgs boson, and the Nature in general at an unprecedented short-distance scales. In this paper, we would like to explore the Higgs physics and examine the accuracies for the electroweak couplings of the Higgs boson at the future high-energy muon collider.

The rest of the paper is organized as follows. We first present the Higgs boson production rates via various production mechanisms at a high-energy muon collider in Sec. 2. We then evaluate the statistical accuracy achievable to determine the HVV couplings in Sec. 3. Foremost, we show the improvement for the precision measurement on the triple Higgs boson coupling as well as the $VVHH$ coupling in Sec. 4. We summarize our results and conclude in Sec. 5.

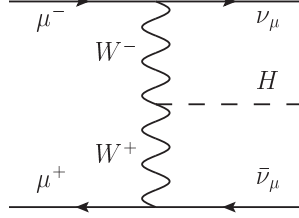


Figure 1: VBF production of a single Higgs boson at a high energy muon collider via WW fusion. For ZZ fusion, replace the W propagator by the Z propagator and the outgoing neutrinos by muons.

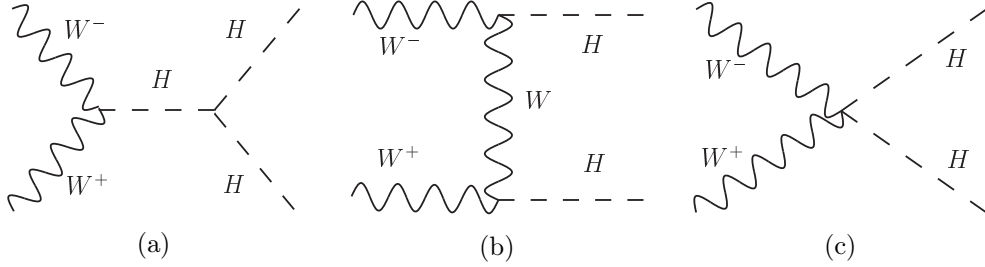


Figure 2: Double Higgs production at a high energy muon collider via WW fusion. The production goes through the VBF topology, as in Fig. 1.

2 Higgs Boson Production at a High-energy Muon Collider

The Higgs boson couples predominantly to heavier particles. The production of a Higgs boson thus involves other heavy particles in the SM. At high energies, gauge bosons will copiously radiate off the colliding beams. Therefore, the vector boson fusion (VBF) mechanism are the dominant source for the Higgs boson production at a high-energy muon collider [29, 30]. The production processes involving the Higgs boson at a high-energy muon collider include

$$\mu^+\mu^- \xrightarrow{\text{VBF}} H, ZH, HH \text{ and } t\bar{t}H, \quad (2.1)$$

which are all dominantly from the VBF processes. We list the production cross sections in Table 1 for those Higgs production processes with a few representative benchmark energy choices. Cross sections are computed using the package **MadGraph** [34]. Recently it has been advocated that, in high energy collisions, it may be appropriate to adopt the approach of electroweak parton distribution functions (EW PDF) [30] to resum the potentially large collinear logarithms at high scales. For the processes under consideration, the difference is insignificant since the single Higgs production is set by a low scale m_H , while the Higgs pair production HH is dominated by the longitudinal gauge boson fusion ($W_L W_L$), that has no scale dependence at the leading order.

We will examine the precision measurements of the Higgs boson couplings via the production processes as depicted in Figs. 1 and 2. For instance, at a 10 TeV muon collider with

\sqrt{s} (TeV)	3	6	10	14	30
benchmark lumi (ab^{-1})	1	4	10	20	90
σ (fb): $WW \rightarrow H$	490	700	830	950	1200
$ZZ \rightarrow H$	51	72	89	96	120
$WW \rightarrow HH$	0.80	1.8	3.2	4.3	6.7
$ZZ \rightarrow HH$	0.11	0.24	0.43	0.57	0.91
$WW \rightarrow ZH$	9.5	22	33	42	67
$WW \rightarrow t\bar{t}H$	0.012	0.046	0.090	0.14	0.28
$WW \rightarrow Z$	2200	3100	3600	4200	5200
$WW \rightarrow ZZ$	57	130	200	260	420

Table 1: SM Higgs boson production cross sections in units of fb at a muon collider for various energies. For comparison, the SM background processes of Z and ZZ production are also shown.

an integrated luminosity of 10 ab^{-1} , we may expect the production of about 10^7 Higgs bosons and 3.6×10^4 Higgs pairs. For comparison, we have also included in Table 1 the SM irreducible backgrounds $\mu^+\mu^- \xrightarrow{\text{VBF}} Z, ZZ$, which are also largely from the VBF mechanism, in Table 1. Although the background rates are larger than the signals by a factor of 4 (55) for the H (HH) process, they populate different kinematical regions from the signals and can be reduced by appropriate kinematic cuts.

3 VVH Couplings

At high energy lepton colliders, the cross section for single H production via the Higgsstrahlung $\mu^+\mu^- \rightarrow ZH$ falls as $1/s$. The high statistics channels for measurements of VVH couplings rely on the WW and ZZ fusion via the VBF topology:

$$\mu^+\mu^- \rightarrow \nu_\mu \bar{\nu}_\mu H \quad (WW \text{ fusion}), \quad (3.1)$$

$$\mu^+\mu^- \rightarrow \mu^+\mu^- H \quad (ZZ \text{ fusion}). \quad (3.2)$$

See Fig. 1 for a representative Feynman diagram. It would be desirable to separate these two classes of events by tagging the outgoing muons and achieve independent measurements on WWH and ZZH couplings. However, for the VBF topology, the outgoing muons have a tendency to stay in the forward region due to the t -channel propagator shown in Fig. 2(a). Although the transverse momentum of the outgoing muons is sizable and governed by the propagator mass $p_T^\mu \sim M_Z$, at very high energies the muons are all extremely forward with a polar angle typically $\theta_\mu \approx M_Z/E_\mu$. In Fig. 3(a), we show the angular distributions of the outgoing muons at $\sqrt{s} = 3, 10, 30 \text{ TeV}$. One can see that, for example, the scattering angle for a muon is peaked near $\theta_\mu \sim 0.02 \approx 1.2^\circ$ at 10 TeV. These very forward muons would most likely escape the detection in a detector at a few degrees away from colliding beams. This

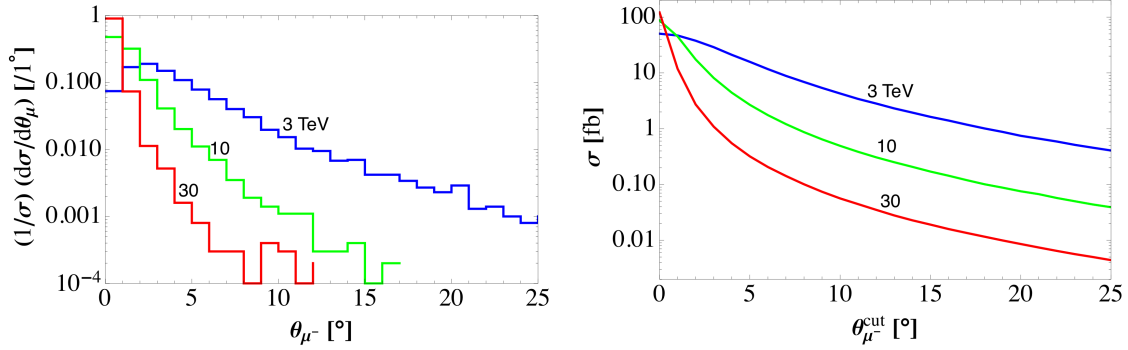


Figure 3: $\mu^+\mu^- \rightarrow \mu^+\mu^-H$ via ZZ fusion with $\sqrt{s} = 3, 10$ and 30 TeV for (a) angular distribution θ_{μ^-} , and (b) total cross section versus an angular cut $\theta_{\mu^-}^{\text{cut}}$.

feature makes it increasingly difficult to distinguish the processes of the neutral currents (ZZ fusion [35]) from the charged currents (WW fusion) at higher energies. Therefore, separating these two classes of events would require the capability of detecting very energetic muons in the forward region of a few degrees with respect to the beam. Without this, we would have to focus on the “inclusiveness,” a dominant behavior of the collinear splitting physics recently emphasized in Ref. [30]. As a consequence, we will consider two classes of events for VBF production of single H :

- Inclusive channel: events from WW fusion and from ZZ fusion without detecting muons;
- Exclusive 1μ channel: events from ZZ fusion with at least one muon detected.

The inclusive channel is populated predominantly by events from the WW fusion, but also contains events from ZZ fusion when the outgoing muons go down the beam pipe and escape detection. However, as seen from Table 1, ZZ -fusion cross section is roughly 10% of the WW fusion cross section, and thus a small contamination for the WWH measurement. The 1μ channel, on the other hand, comes from the ZZ fusion and is uniquely sensitive to the ZZH coupling, although it suffers from poor selection efficiency after requiring a muon identification. In Fig. 3(b), we illustrate the fiducial cross section after the angular acceptance cut $\theta_{\mu^-}^{\text{cut}}$. At a fixed angular acceptance, the cross section falls as $\sigma \sim 1/E_{\mu}^2$.

3.1 Inclusive channel

Processes contributing to the inclusive channel are shown in Eqs. (3.1) and (3.2). We focus on the leading decay channel $H \rightarrow b\bar{b}$. The Higgs boson signal will be $b\bar{b}$ pair near the Higgs mass m_H plus large missing energy, resulting from the missing neutrinos and the undetected muons. We impose the basic acceptance cuts on the b jets

$$p_T(b) > 30 \text{ GeV}, \quad 10^\circ < \theta_b < 170^\circ, \quad (3.3)$$

where θ_b is the polar angle of the $b(\bar{b})$ jet in the lab frame. The irreducible backgrounds, $\mu^+\mu^- \rightarrow \nu_\mu\bar{\nu}_\mu Z$, from either WW fusion shown in Table 1 or $\mu^+\mu^- \rightarrow ZZ \rightarrow \nu_\mu\bar{\nu}_\mu Z$, which can be readily removed due to the on-shell Z decay $Z \rightarrow \nu_\mu\bar{\nu}_\mu$, by a “recoil mass” cut

$$M_{\text{recoil}} = (p_{\mu^+} + p_{\mu^-} - p_H)^2 > 200 \text{ GeV}. \quad (3.4)$$

The key aspect to identify the Higgs signal lies in the resolution to effectively select the $b\bar{b}$ at the resonant m_H . In Fig. 4(a) we plot the invariant mass distribution for the H signal for $\sqrt{s} = 10 \text{ TeV}$, after the acceptance cuts and assuming a jet energy resolution of

$$\Delta E/E = 10\%. \quad (3.5)$$

For comparison, we have also shown in the same plot the distribution from the Z background. Here we have included all quarks flavors b, c, s, d, u . If we demanded a b -tagging for our signal selection, we would be able to reduce the $Z \rightarrow jj$ background by a factor of 5. However, we do not find the b -tagging necessary due to the highly efficient kinematical constraint on $m_{b\bar{b}}$. In estimating the statistical accuracy for the coupling measurement, we impose the a mass cut

$$m_{b\bar{b}} = m_H \pm 15 \text{ GeV}. \quad (3.6)$$

With those cuts, the Z background is essentially removed and we retain the majority of the signal. The event selection efficiencies (ϵ_{in}) and the resulting cross sections at different collider energies are summarized in Table 2 in the top rows.

It is worth noting that, at higher CM energies, the b jets have increasingly small polar angles in the Lab frame and become more forward. The angular distributions for various energies are shown in the right panel of Fig. 4, where we see the majority of b jets have $\theta_b < 10^\circ$ at $\sqrt{s} = 30 \text{ TeV}$. This is the reason for the worsening selection efficiencies in Table 2 as we go to higher CM energies. Obviously, extending the detector angular coverage would significantly increase the signal acceptance. If the angular cut on θ_b in Eq. (3.3) is tightened up to $20^\circ - 160^\circ$ instead, the signal reconstruction efficiency will be scaled down by about 10%.

The total cross section in the inclusive channel can be written, at the leading order, as

$$\sigma_{\text{in}} = (1 + \Delta\kappa_W)^2 \sigma_W^{\text{SM}} + (1 + \Delta\kappa_Z)^2 \sigma_Z^{\text{SM}} \quad (3.7)$$

where σ_W^{SM} and σ_Z^{SM} are the SM cross sections for the WW/ZZ fusion processes. In cases where $\Delta\kappa_{W/Z} \ll 1$, the linear terms dominate which, in the EFT language, is equivalent to keeping only the interference term from the dim-6 operators. We do not make such an assumption in the κ -scheme adopted in this work.

In this subsection we will vary κ_W and κ_Z one at a time, and consider a simultaneous fit to both parameters later in this section. The 95% confidence level (C.L.) sensitivities in the relative errors $\Delta\kappa_{W/Z}$ are shown in Table 3. The achievable accuracies are impressive, comparing with the anticipated best results $\Delta\kappa_W \sim 0.6\%$ from the ILC/CLIC and $\Delta\kappa_Z \sim 0.2\%$ from the expectations at the Higgs factories [15, 17].

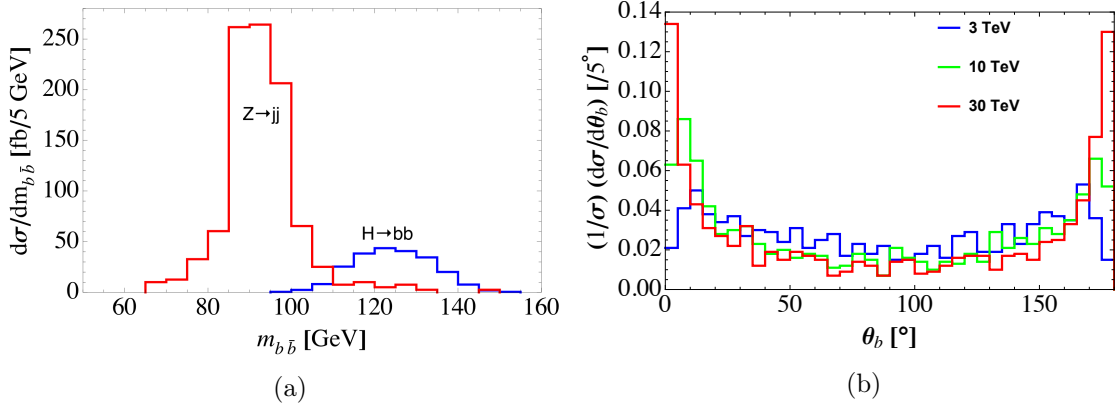


Figure 4: (a) Invariant mass distribution for the Higgs boson and Z boson at $\sqrt{s} = 10$ TeV with an energy resolution 10%, and (b) the b -quark angular distribution θ_b in the lab frame for $\sqrt{s} = 3, 10, 30$ TeV.

\sqrt{s} (TeV)	3	6	10	14	30
$WW \rightarrow H : \epsilon_{\text{in}} (\%)$	54	46	42	39	32
$ZZ \rightarrow H : \epsilon_{\text{in}} (\%)$	57	49	44	41	35
Cross section σ_{in} (fb)	170	200	220	240	240
$ZZ \rightarrow H : \epsilon_{1\mu} (\%)$	11	2.7	0.84	0.37	0.071
Cross section $\sigma_{1\mu}$ (fb)	3.1	1.1	0.43	0.20	0.050
$VV \rightarrow HH : \epsilon_{hh} (\%)$	27	18	13	11	7.2
Cross section σ_{hh} (ab)	81	140	150	170	200

Table 2: Selection efficiencies and the estimated cross sections after selection cuts for the inclusive channel, exclusive 1μ channel, as well as the inclusive HH channel.

\sqrt{s} (TeV)	3	6	10	14	30
benchmark lumi (ab^{-1})	1	4	10	20	90
$(\Delta\kappa_W)_{\text{in}}$	0.26%	0.12%	0.073%	0.050%	0.023%
$(\Delta\kappa_Z)_{\text{in}}$	2.4%	1.1%	0.65%	0.46%	0.20%
$(\Delta\kappa_Z)_{1\mu}$	1.7%	1.5%	1.5%	1.5%	1.5%

Table 3: The 95% C.L. in $\Delta\kappa_{W/Z}$ in the inclusive channel by varying one coupling at a time, as well as for $\Delta\kappa_Z$ from the exclusive 1μ process.

3.2 Exclusive 1μ channel

The leading process contributing to the exclusive 1μ channel is ZZ fusion in Eq. (3.2), whose rate is shown in Table 1. Again, with the same decay mode, the Higgs boson signal will be $b\bar{b}$ pair near the Higgs mass m_H plus $\mu^+\mu^-$ in the forward-backward regions. The leading

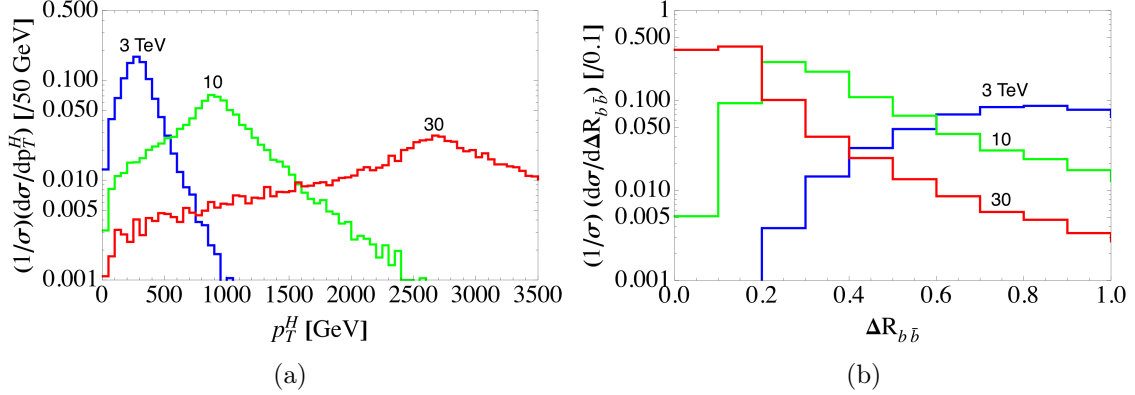


Figure 5: (a) p_T^H distribution of the Higgs boson in 1μ channel (b) Separation of the b jets from $H \rightarrow b\bar{b}$.

background is $\mu^+\mu^- \rightarrow ZZ \rightarrow \mu^+\mu^-Z$ with $Z \rightarrow b\bar{b}$. There is no WW fusion analogue for this channel. We adopt the same basic cuts as in Eqs. (3.3), (3.4) and (3.6). The background is highly suppressed. In addition, we require the presence of at least one muon to be in

$$10^\circ < \theta_{\mu^\pm} < 170^\circ. \quad (3.8)$$

This turns out to be very costly to the signal, since the majority of the muons have $\theta_\mu < 10^\circ$, as already seen in Fig. 3. As such, the signal reconstruction efficiencies for this channel are very low and are shown in Table 2, together with the predicted cross sections in the middle rows. With the high luminosity expected, the 95% C.L. on the coupling measurements is shown also in Table 3 for the exclusive 1μ channel. Although the result at a 3 TeV collider is comparable to that from the inclusive channel, at higher energies the estimated precision is worse than the inclusive channel despite the higher energies and more luminosities. This is mainly due to the significantly reduced number of events from the tagging requirement for a forward-backward muon.

It is important to note another significant consequence of requiring one muon in the range of $10^\circ < \theta_{\mu^\pm} < 170^\circ$. For highly energetic muons, this large scattering angle leads to a high transverse momentum $p_T^\mu > 0.17E_\mu$ and, consequently, induces a strong recoil in the Higgs boson produced in the final state. In Fig. 5 we show the p_T distribution of the Higgs boson in (a) for the 1μ channel as well as R_{bb} in (b), the separation of the b -jets from $H \rightarrow b\bar{b}$. In particular, at $\sqrt{s} = 30$ TeV, the Higgs boson tend to have a large p_T , in the order of 2.5 TeV, and the resulting decay is boosted with $R_{bb} \sim 0.2$. Care needs to be taken when reconstructing such boosted events.

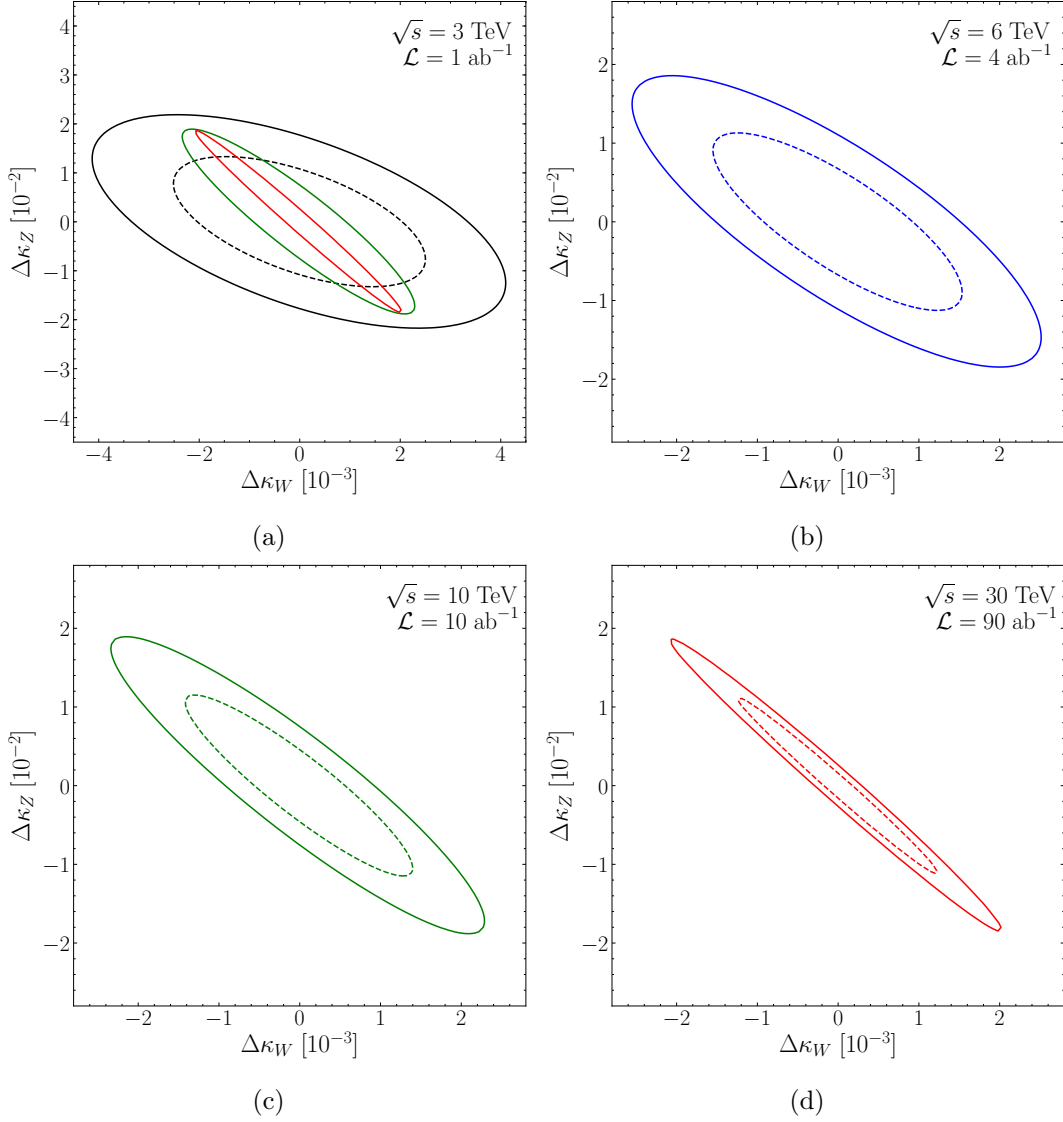


Figure 6: Correlated bounds with 95% C.L. (solid) and 68% C.L. (dashed) in the $\Delta\kappa_W$ - $\Delta\kappa_Z$ plane for $\sqrt{s} = 3, 6, 10, 30$ TeV, respectively. In (a), inner ellipses (solid) include the 95% C.L. results for 10 TeV and 30 TeV for comparison.

3.3 Two-parameter likelihood fit of κ_W and κ_Z

In this subsection we perform a two-bin likelihood fit of κ_W and κ_Z making use of the inclusive and exclusive 1μ channels. We construct a Poisson log-likelihood function

$$\text{LL} = \ln \frac{e^{-N(\Delta\kappa_W, \Delta\kappa_Z)} [N(\Delta\kappa_W, \Delta\kappa_Z)]^{N_{\text{SM}}}}{N_{\text{SM}}!}, \quad (3.9)$$

where the numbers of events are

$$N(\Delta\kappa_W, \Delta\kappa_Z) = \sigma(\Delta\kappa_W, \Delta\kappa_Z) \mathcal{L}_{\text{lumi}} , \quad N_{\text{SM}} = \sigma(\Delta\kappa_W = 0, \Delta\kappa_Z = 0) \mathcal{L}_{\text{lumi}} , \quad (3.10)$$

and $\mathcal{L}_{\text{lumi}}$ is the integrated luminosity. We compute such likelihood function for each channel and a global likelihood as the product of the individual ones. Then we compute the 68% and 95% C.L. regions on the $\Delta\kappa_W$ - $\Delta\kappa_Z$ plane, corresponding to $\text{LL} = \text{LL}_{\text{max}} - 1.15$ and $\text{LL} = \text{LL}_{\text{max}} - 3.10$, respectively. The resulting contours are shown in Fig. 6. As expected, the precision for $\Delta\kappa_W$ is better than $\Delta\kappa_Z$ by about an order of magnitude at high energies. The projection of the ellipses onto the $\Delta\kappa_W$ -axis in Fig. 6 gives the uncertainty marginalized over $\Delta\kappa_Z$, and vice versa. The resulting errors are larger than those in the single parameter fit, which varies one parameter at a time and assumes SM values for the rest.

4 HHH and $WWHH$ Couplings

Pair production of the Higgs boson provides a direct measurement on the trilinear HHH and quartic $VVHH$ couplings. The main advantage of a high-energy collider, with $\sqrt{s} \gg 2m_H$, lies in the capability to copiously produce Higgs boson pairs. At a high-energy muon collider, as shown in Sec. 2, one would expect about 36,000 (68,000) HH at 10 TeV (30 TeV). To probe the Higgs self-coupling, we utilize the VBF mechanism for the inclusive double Higgs production

$$\mu^+ \mu^- \xrightarrow{VBF} HH + X , \quad (4.1)$$

where $X = \nu\bar{\nu}$ for WW fusion and $\mu^+ \mu^-$ for the ZZ fusion. As can be seen from the Feynman diagrams in Fig. 2, the HH production involves three classes of couplings: κ_W, κ_3 and κ_{W2} . Since κ_W can be measured very precisely from the single Higgs production, as shown in Section 3, we will assume in the current section that $\kappa_W = 1$ as in the SM and study the interplay of κ_3 and κ_{W2} in the HH production. As discussed in Section 3, the outgoing remnant particles tend to stay in the forward region and escape detection. Therefore, similar to the single Higgs production, we will consider the inclusive channel in Eq. (4.1), which is populated dominantly by the WW fusion and, to a less extent, by the ZZ fusion events when the outgoing muons are too forward to be detected.

The cross section for the inclusive $\mu^+ \mu^- \rightarrow HH + X$ can be parametrized as [36]

$$\sigma = \sigma_{\text{SM}} \left[1 + R_1 \Delta\kappa_{W2} + R_2 \Delta\kappa_3 + R_3 \Delta\kappa_{W2} \Delta\kappa_3 + R_4 (\Delta\kappa_{W2})^2 + R_5 (\Delta\kappa_3)^2 \right] , \quad (4.2)$$

where the σ_{SM} is the SM cross section. The SM cross section σ_{SM} and coefficients R_i , before any cuts, are given in Table 4. It is instructive to consider the energy dependence of different classes of Feynman diagrams contributing to HH production, by studying the partonic scattering $W^+ W^- \rightarrow HH$. As the dominant contribution comes from the longitudinal W scattering $W_L^+ W_L^- \rightarrow HH$, the scattering amplitude can be written as

$$\mathcal{A}(W_L^+ W_L^- \rightarrow HH) = \mathcal{A}_{\text{SM}} + \mathcal{A}_1 \Delta\kappa_{W2} + \mathcal{A}_2 \Delta\kappa_3 , \quad (4.3)$$

\sqrt{s} [TeV]	σ_{SM} [fb]	R_1	R_2	R_3	R_4	R_5
3 TeV	0.91	-3.5	-0.65	3.1	14	0.49
6 TeV	2.0	-3.9	-0.50	2.8	29	0.35
10 TeV	3.6	-4.3	-0.43	2.7	54	0.29
14 TeV	4.9	-4.4	-0.38	2.6	80	0.25
30 TeV	7.6	-4.4	-0.28	2.3	210	0.19

Table 4: Predicted cross sections of the inclusive $\mu^+\mu^- \rightarrow HH + X$, as given in Eq. (4.2) at different muon collider energies.

where \mathcal{A}_{SM} , $\mathcal{A}_2 \sim \text{constant}$, and $\mathcal{A}_1 \sim E^2$ at high energies $E \gg M_W$. Because of the energy growing behavior of \mathcal{A}_1 , the cross section has a strong dependence on $\Delta\kappa_{W_2}$ over a large range of phase space. As a result, we expect to be able to constrain κ_{W_2} better than κ_3 . This argument also shows, when extracting the trilinear Higgs self-coupling it is important to consider the impact from the quartic $VVHH$ coupling. In this study, we have assumed the $HHVV$ vertex is modified only in its strength for simplicity, while in many well-motivated new physics models the tensor structure of the quartic coupling could also be corrected [37, 38]. It will be interesting to further assess the impact of these additional modifications on the extraction of κ_3 [39].

For the Higgs decays, we once again focus on the leading decay channel $HH \rightarrow b\bar{b} b\bar{b}$, which has a SM branching fraction $\text{BR}(4b) \simeq 34\%$. We impose basic acceptance cuts

$$p_T(b) > 30 \text{ GeV}, \quad 10^\circ < \theta_b < 170^\circ, \quad \Delta R_{bb} > 0.4. \quad (4.4)$$

As before, we further assume the jet energy resolution to be $\Delta E/E = 10\%$.

The Higgs candidates are reconstructed from the four most energetic jets. The four jets are paired by minimizing

$$(m_{j_1 j_2} - m_H)^2 + (m_{j_3 j_4} - m_H)^2. \quad (4.5)$$

And for each Higgs candidate, we impose

$$|m_{jj} - m_H| < 15 \text{ GeV} \quad (4.6)$$

to reject background from Z and W resonances. We also require the recoil mass

$$M_{\text{recoil}} = \sqrt{(p_{\mu^+} + p_{\mu^-} - p_{H_1} - p_{H_2})^2} > 200 \text{ GeV}. \quad (4.7)$$

The signal selection efficiencies and the corresponding cross sections are listed in Table 2. If we tighten the angular cut to 20° , the efficiencies would drop by a factor of 3–4.

We again perform a simultaneous fit to κ_3 and κ_{W_2} using binned maximum likelihood fit. Given the different energy dependence in the subamplitudes controlled by κ_3 and κ_{W_2} , we decided to bin the m_{HH} distribution into the following intervals²

$$m_{HH} = [0, 350, 450, 550, 650, 750, 950, 1350, 5000] \text{ GeV}. \quad (4.8)$$

²A similar procedure for double Higgs production in hadron colliders can be found in Ref. [40].

m_{HH} [GeV]	σ_{SM} [ab]	r_1	r_2	r_3	r_4	r_5
[0, 350)	15	-2.7	-1.7	7.6	6.7	2.6
[350, 450)	24	-3.4	-1.2	5.2	7.8	0.95
[450, 550)	24	-4.0	-0.91	4.6	12	0.52
[550, 650)	21	-4.6	-0.70	4.7	17	0.36
[650, 750)	17	-5.3	-0.60	5.1	26	0.28
[750, 950)	24	-6.9	-0.52	6.3	46	0.23
[950, 1350)	23	-11	-0.47	8.7	120	0.19
[1350, 5000)	15	-18	-0.30	7.2	240	0.075

Table 5: Cross sections of the inclusive $\mu^+\mu^- \rightarrow HH + X \rightarrow b\bar{b} b\bar{b} + X$ in different m_{HH} ranges as the coefficients corresponding to the five terms in Eq. (4.9) with $\sqrt{s} = 10$ TeV.

\sqrt{s} (TeV)	3	6	10	14	30
benchmark lumi (ab ⁻¹)	1	4	10	20	90
$(\Delta\kappa_{W_2})_{\text{in}}$	5.3%	1.3%	0.62%	0.41%	0.20%
$(\Delta\kappa_3)_{\text{in}}$	25%	10%	5.6%	3.9%	2.0%

Table 6: The 95% C.L. in $\Delta\kappa_{W_2}$ and $\Delta\kappa_3$ for the inclusive channel, by varying one coupling at a time.

The binned cross section of $\mu^+\mu^- \rightarrow HH + X \rightarrow b\bar{b} b\bar{b} + X$ after the selection cuts can be parametrized, in a similar fashion, as

$$\sigma = \sigma_{\text{SM}} \left[1 + r_1 \Delta\kappa_{W_2} + r_2 \Delta\kappa_3 + r_3 \Delta\kappa_{W_2} \Delta\kappa_3 + r_4 (\Delta\kappa_{W_2})^2 + r_5 (\Delta\kappa_3)^2 \right], \quad (4.9)$$

where the values are given in Table 5 for $\sqrt{s} = 10$ TeV for illustration. It is important to note again the increasing sensitivity on κ_{W_2} at higher values of m_{HH} . The resulting contours are shown in Fig. 7. In Table 6 we also provide the 95% C.L. from the single parameter fit, by allowing κ_3 and κ_{W_2} to vary only one at a time.

5 Discussion and Conclusion

As we have shown in this work, a multi-TeV high energy muon collider will have a tremendous potential to constrain the electroweak Higgs couplings with unprecedented accuracy. It will offer a unique probe into the nature of the Higgs boson as well as the scale of possible new physics beyond the SM. In Table 7, we present a summary of the estimated sensitivities at different collider energies and luminosities. In the last column of the table, we compare with the expected precision from other proposed colliders. It is clear that a multi-TeV muon collider could improve the measurements substantially.

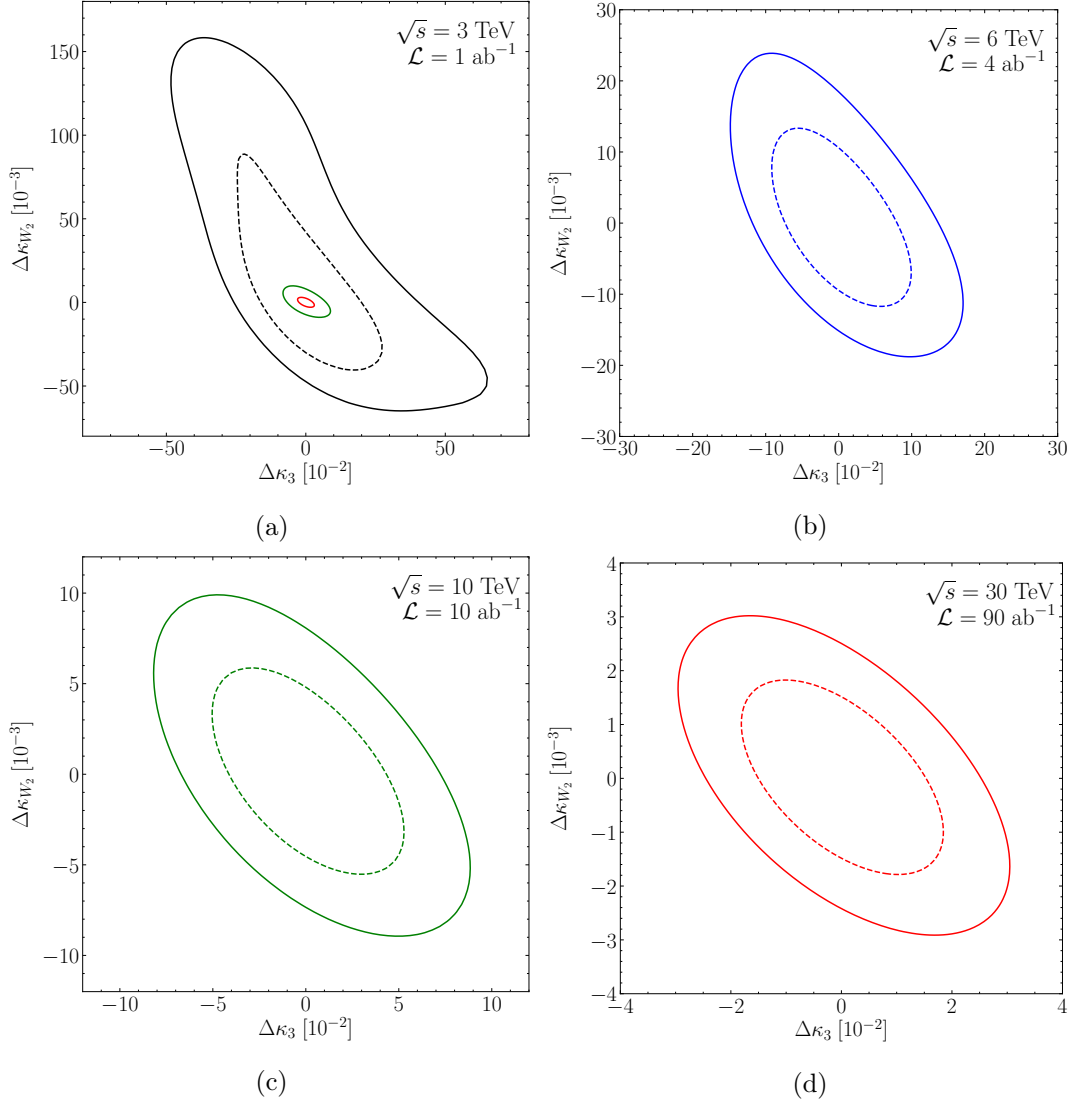


Figure 7: Correlated bounds with 95% C.L. (solid) and 68% C.L. (dashed) in the $\Delta\kappa_{W_2}$ - $\Delta\kappa_3$ plane for $\sqrt{s} = 3, 6, 10, 30$ TeV, respectively. In (a), inner ellipses (solid) include the 95% C.L. results for 10 TeV and 30 TeV for comparison.

It is possible to translate the bound in the κ -scheme into the constraint on Λ , the scale of new physics associated with the dim-6 operators in Eq. (1.2),

$$\Lambda \sim \sqrt{\frac{c_{H,6}}{\Delta\kappa}} v. \quad (5.1)$$

Assuming $c_{6,H} \sim \mathcal{O}(1)$, the scale is estimated to be $\Lambda \sim 1 \text{ TeV}/\sqrt{16\Delta\kappa}$, as shown in Table 7. A summary figure, which combines our results for the coupling measurements, is given in Fig. 8, with the upper horizontal axis marking the estimated scale Λ in TeV. With $\Lambda/\sqrt{c_i} \sim (10 - 16)$

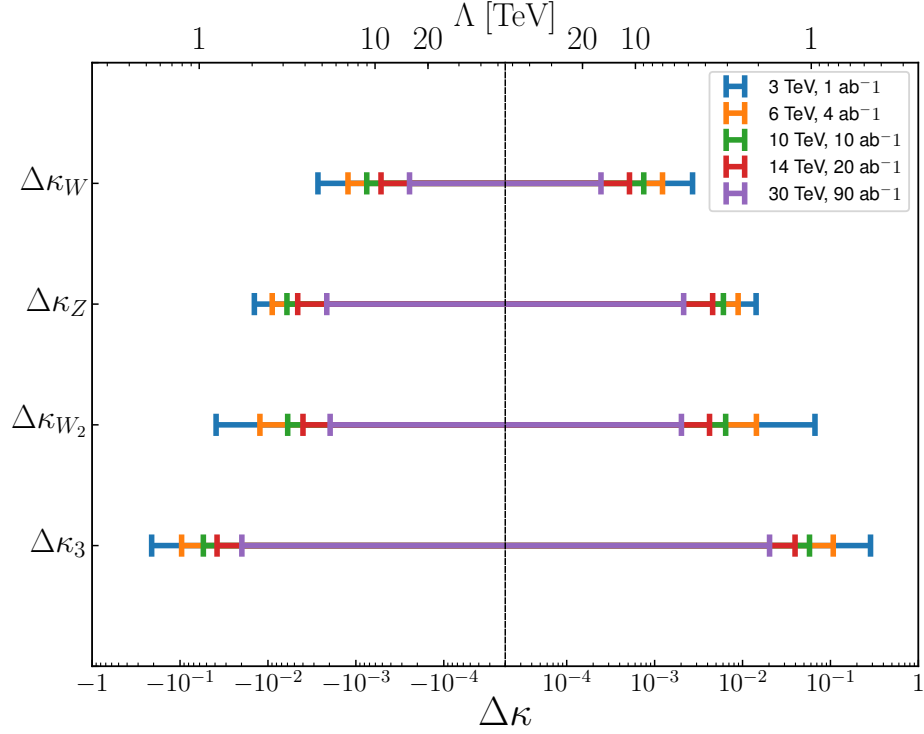


Figure 8: Summary of the expected accuracies at 95% C.L. for the Higgs couplings at a variety of muon collider collider energies and luminosities. The upper horizontal axis marks the accessible scale Λ , assuming $c_{6,H} \sim \mathcal{O}(1)$.

TeV at a collider of (10 – 30) TeV, we would be probing new physics at very high scales or deeply into quantum effects.

\sqrt{s} (lumi.)	3 TeV (1 ab ⁻¹)	6 (4)	10 (10)	14 (20)	30 (90)	Comparison
WWH ($\Delta\kappa_W$)	0.26%	0.12%	0.073%	0.050%	0.023%	0.1% [41]
$\Lambda/\sqrt{c_i}$ (TeV)	4.7	7.0	9.0	11	16	(68% C.L.)
ZZH ($\Delta\kappa_Z$)	1.4%	0.89%	0.61%	0.46%	0.21%	0.13% [17]
$\Lambda/\sqrt{c_i}$ (TeV)	2.1	2.6	3.2	3.6	5.3	(95% C.L.)
$WWHH$ ($\Delta\kappa_{W_2}$)	5.3%	1.3%	0.62%	0.41%	0.20%	5% [36]
$\Lambda/\sqrt{c_i}$ (TeV)	1.1	2.1	3.1	3.8	5.5	(68% C.L.)
HHH ($\Delta\kappa_3$)	25%	10%	5.6%	3.9%	2.0%	5% [22, 23]
$\Lambda/\sqrt{c_i}$ (TeV)	0.49	0.77	1.0	1.2	1.7	(68% C.L.)

Table 7: Summary table of the expected accuracies at 95% C.L. for the Higgs couplings at a variety of muon collider collider energies and luminosities.

In our analyses, we only focused on the leading decay channel $H \rightarrow b\bar{b}$. A more com-

prehensive study could include the other decay channels as well, such as $H \rightarrow, WW, ZZ, \tau\tau$ and $\gamma\gamma$, to further improve the precision. On the other hand, due to the lack of knowledge of the specifics of the detector design, we have not made any attempts for experimental detector simulations. Further work may be needed to draw a more complete conclusion for the expected sensitivity reach.

In summary, we estimated the expected precision at a multi-TeV muon collider for measuring the Higgs boson couplings with electroweak gauge bosons, HVV and $HHVV$, as well as the trilinear Higgs self-coupling HHH . With the anticipated high CM energies and high luminosities, a multi-TeV muon collider could provide us with unparalleled precision for Higgs physics and, consequently, offer some of the most stringent experimental tests of the SM Higgs sector. As we have shown in this study, the outgoing remnant particles have a strong tendency to stay in the very forward region. The enhanced collinear behavior of the final state particles results in the dominant configuration of “inclusive” processes, a notion usually reserved for hadron colliders, unless there is a device to detect the very forward muons of a few degrees from the beam. These features add new subtlety to Higgs coupling measurements, since it is now difficult to isolate WW fusion from ZZ fusion events in the Higgs production. We addressed the subtlety by performing binned maximum likelihood analyses to simultaneously fit two parameters involved in the inclusive processes. The approach and methodology adopted in this study could be applicable to new physics searches at a high energy muon collider.

Acknowledgments

The work of TH was supported in part by the U.S. Department of Energy under grant No. DE-FG02-95ER40896 and in part by the PITT PACC. The work of DL was supported in part by the U.S. Department of Energy under grant DE-SC-0009999. IL is supported in part by the U.S. Department of Energy under contracts No. DE-AC02-06CH11357 at Argonne and No. DE-SC0010143 at Northwestern. XW was supported by the National Science Foundation under Grant No. PHY-1915147.

References

- [1] P. Sikivie, L. Susskind, M. B. Voloshin, and V. I. Zakharov, “Isospin Breaking in Technicolor Models,” *Nucl. Phys. B* **173** (1980) 189–207.
- [2] **ALEPH, DELPHI, L3, OPAL, SLD, LEP Electroweak Working Group, SLD Electroweak Group, SLD Heavy Flavour Group** Collaboration, S. Schael *et al.*, “Precision electroweak measurements on the Z resonance,” *Phys. Rept.* **427** (2006) 257–454, [arXiv:hep-ex/0509008](#).
- [3] B. Grzadkowski, M. Iskrzynski, M. Misiak, and J. Rosiek, “Dimension-Six Terms in the Standard Model Lagrangian,” *JHEP* **10** (2010) 085, [arXiv:1008.4884 \[hep-ph\]](#).
- [4] V. Barger, T. Han, P. Langacker, B. McElrath, and P. Zerwas, “Effects of genuine dimension-six Higgs operators,” *Phys. Rev. D* **67** (2003) 115001, [arXiv:hep-ph/0301097](#).

- [5] G. Giudice, C. Grojean, A. Pomarol, and R. Rattazzi, “The Strongly-Interacting Light Higgs,” *JHEP* **06** (2007) 045, [arXiv:hep-ph/0703164](#).
- [6] I. Low, R. Rattazzi, and A. Vichi, “Theoretical Constraints on the Higgs Effective Couplings,” *JHEP* **04** (2010) 126, [arXiv:0907.5413 \[hep-ph\]](#).
- [7] X. Zhang, “Operator analysis for the higgs potential and cosmological bound on the higgs-boson mass,” *Physical Review D* **47** no. 7, (Apr, 1993) 3065–3067.
<http://dx.doi.org/10.1103/PhysRevD.47.3065>.
- [8] C. Grojean, G. Servant, and J. D. Wells, “First-order electroweak phase transition in the standard model with a low cutoff,” *Physical Review D* **71** no. 3, (Feb, 2005) .
<http://dx.doi.org/10.1103/PhysRevD.71.036001>.
- [9] X. Gan, A. J. Long, and L.-T. Wang, “Electroweak sphaleron with dimension-six operators,” *Physical Review D* **96** no. 11, (Dec, 2017) .
<http://dx.doi.org/10.1103/PhysRevD.96.115018>.
- [10] **ATLAS** Collaboration, G. Aad *et al.*, “Combined measurements of Higgs boson production and decay using up to 80 fb⁻¹ of proton-proton collision data at $\sqrt{s} = 13$ TeV collected with the ATLAS experiment,” *Phys. Rev. D* **101** no. 1, (2020) 012002, [arXiv:1909.02845 \[hep-ex\]](#).
- [11] **CMS** Collaboration, A. M. Sirunyan *et al.*, “Combined measurements of Higgs boson couplings in proton–proton collisions at $\sqrt{s} = 13$ TeV,” *Eur. Phys. J. C* **79** no. 5, (2019) 421, [arXiv:1809.10733 \[hep-ex\]](#).
- [12] M. Cepeda *et al.*, *Report from Working Group 2: Higgs Physics at the HL-LHC and HE-LHC*, vol. 7, pp. 221–584. 12, 2019. [arXiv:1902.00134 \[hep-ph\]](#).
- [13] D. Asner *et al.*, “ILC Higgs White Paper,” in *Community Summer Study 2013: Snowmass on the Mississippi*. 10, 2013. [arXiv:1310.0763 \[hep-ph\]](#).
- [14] **ILD** Collaboration, J. Tian and K. Fujii, “Measurement of Higgs couplings and self-coupling at the ILC,” *PoS EPS-HEP2013* (2013) 316, [arXiv:1311.6528 \[hep-ph\]](#).
- [15] **FCC** Collaboration, A. Abada *et al.*, “FCC-ee: The Lepton Collider: Future Circular Collider Conceptual Design Report Volume 2,” *Eur. Phys. J. ST* **228** no. 2, (2019) 261–623.
- [16] **CEPC Study Group** Collaboration, M. Dong *et al.*, “CEPC Conceptual Design Report: Volume 2 - Physics & Detector,” [arXiv:1811.10545 \[hep-ex\]](#).
- [17] F. An, Y. Bai, C. Chen, X. Chen, Z. Chen, J. G. da Costa, Z. Cui, Y. Fang, C. Fu, J. Gao, and *et al.*, “Precision higgs physics at the cepec,” *Chinese Physics C* **43** no. 4, (Apr, 2019) 043002.
<http://dx.doi.org/10.1088/1674-1137/43/4/043002>.
- [18] A. Robson and P. Roloff, “Updated CLIC luminosity staging baseline and Higgs coupling prospects,” [arXiv:1812.01644 \[hep-ex\]](#).
- [19] **CLICdp** Collaboration, P. Roloff, U. Schnoor, R. Simoniello, and B. Xu, “Double Higgs boson production and Higgs self-coupling extraction at CLIC,” [arXiv:1901.05897 \[hep-ex\]](#).
- [20] V. D. Barger and T. Han, “Double Higgs Boson Production via WW Fusion in TeV e^+e^- Collisions,” *Mod. Phys. Lett. A* **5** (1990) 667–674.
- [21] W. Kilian, S. Sun, Q.-S. Yan, X. Zhao, and Z. Zhao, “Multi-Higgs boson production and

- unitarity in vector-boson fusion at future hadron colliders,” *Phys. Rev. D* **101** no. 7, (2020) 076012, [arXiv:1808.05534 \[hep-ph\]](#).
- [22] FCC Collaboration, A. Abada *et al.*, “FCC-hh: The Hadron Collider: Future Circular Collider Conceptual Design Report Volume 3,” *Eur. Phys. J. ST* **228** no. 4, (2019) 755–1107.
- [23] M. Ahmad *et al.*, “CEPC-SPPC Preliminary Conceptual Design Report. 1. Physics and Detector,” tech. rep., 3, 2015.
- [24] M. Chiesa, F. Maltoni, L. Mantani, B. Mele, F. Piccinini, and X. Zhao, “Measuring the quartic Higgs self-coupling at a multi-TeV muon collider,” [arXiv:2003.13628 \[hep-ph\]](#).
- [25] S. Gori and I. Low, “Precision Higgs Measurements: Constraints from New Oblique Corrections,” *JHEP* **09** (2013) 151, [arXiv:1307.0496 \[hep-ph\]](#).
- [26] J. P. Delahaye, M. Diemoz, K. Long, B. Mansouli, N. Pastrone, L. Rivkin, D. Schulte, A. Skrinsky, and A. Wulzer, “Muon Colliders,” [arXiv:1901.06150 \[physics.acc-ph\]](#).
- [27] K. Long, D. Lucchesi, M. Palmer, N. Pastrone, D. Schulte, and V. Shiltsev, “Muon Colliders: Opening New Horizons for Particle Physics,” [arXiv:2007.15684 \[physics.acc-ph\]](#).
- [28] D. Buttazzo, D. Redigolo, F. Sala, and A. Tesi, “Fusing Vectors into Scalars at High Energy Lepton Colliders,” *JHEP* **11** (2018) 144, [arXiv:1807.04743 \[hep-ph\]](#).
- [29] A. Costantini, F. De Lillo, F. Maltoni, L. Mantani, O. Mattelaer, R. Ruiz, and X. Zhao, “Vector boson fusion at multi-TeV muon colliders,” 5, 2020. [arXiv:2005.10289 \[hep-ph\]](#).
- [30] T. Han, Y. Ma, and K. Xie, “High Energy Leptonic Collisions and Electroweak Parton Distribution Functions,” [arXiv:2007.14300 \[hep-ph\]](#).
- [31] R. Capdevilla, D. Curtin, Y. Kahn, and G. Krnjaic, “A Guaranteed Discovery at Future Muon Colliders,” [arXiv:2006.16277 \[hep-ph\]](#).
- [32] V. D. Barger, M. Berger, J. Gunion, and T. Han, “s channel Higgs boson production at a muon muon collider,” *Phys. Rev. Lett.* **75** (1995) 1462–1465, [arXiv:hep-ph/9504330](#).
- [33] V. D. Barger, M. Berger, J. Gunion, and T. Han, “Higgs Boson physics in the s channel at $\mu^+\mu^-$ colliders,” *Phys. Rept.* **286** (1997) 1–51, [arXiv:hep-ph/9602415](#).
- [34] J. Alwall, R. Frederix, S. Frixione, V. Hirschi, F. Maltoni, O. Mattelaer, H. S. Shao, T. Stelzer, P. Torrielli, and M. Zaro, “The automated computation of tree-level and next-to-leading order differential cross sections, and their matching to parton shower simulations,” *JHEP* **07** (2014) 079, [arXiv:1405.0301 \[hep-ph\]](#).
- [35] T. Han, Z. Liu, Z. Qian, and J. Sayre, “Improving Higgs Coupling Measurements Through ZZ Fusion at the ILC,” *Phys. Rev. D* **91** (2015) 113007, [arXiv:1504.01399 \[hep-ph\]](#).
- [36] R. Contino, C. Grojean, D. Pappadopulo, R. Rattazzi, and A. Thamm, “Strong Higgs Interactions at a Linear Collider,” *JHEP* **02** (2014) 006, [arXiv:1309.7038 \[hep-ph\]](#).
- [37] D. Liu, I. Low, and Z. Yin, “Universal Imprints of a Pseudo-Nambu-Goldstone Higgs Boson,” *Phys. Rev. Lett.* **121** no. 26, (2018) 261802, [arXiv:1805.00489 \[hep-ph\]](#).
- [38] D. Liu, I. Low, and Z. Yin, “Universal Relations in Composite Higgs Models,” *JHEP* **05** (2019) 170, [arXiv:1809.09126 \[hep-ph\]](#).
- [39] T. Han, D. Liu, I. Low, and X. Wang, work in progress.

- [40] C.-R. Chen and I. Low, “Double take on new physics in double Higgs boson production,” *Phys. Rev. D* **90** no. 1, (2014) 013018, [arXiv:1405.7040 \[hep-ph\]](#).
- [41] R. Franceschini *et al.*, “The CLIC Potential for New Physics,” [arXiv:1812.02093 \[hep-ph\]](#).